Curli fibers in *Escherichia coli* biofilms: the influence of water availability on amyloid structure and properties

Macarena Siri[1]*, Agustín Mangiarotti[2], Mónica Vázquez-Dávila[1], Cécile M. Bidan[1]

[1] *Max Planck Institute of Colloids and Interfaces, Department of Biomaterials, Potsdam, Germany*

[2] *Max Planck Institute of Colloids and Interfaces, Department of Colloids, Potsdam, Germany*

ABSTRACT: Microbial biofilms are multicellular communities where bacteria produce an extracellular matrix mainly consisting of proteins and polysaccharides. These biofilms not only confer resistance against external stresses (e.g. antibiotics), but their physical and chemical properties can also adapt to environmental conditions (e.g. temperature, humidity, etc.). Gaining insight on how such cues affect the molecular structure of biofilms would greatly benefit to the emerging field of engineered living materials. In this work, we studied the physical-chemical properties of curli amyloid fibers extracted from biofilms grown on substrates with different water contents. Electron microscopy, FT-IR and fluorescence spectroscopy were used to characterize the conformation and physical-chemical properties of these fibers as a function of the biofilm growth conditions. The results show that varying the water content of the substrate leads to differences in the yield of curli fibers purified from the biofilms and to differences in the packing, hydrophobic character and chemical stability of the fibers. Fibers from biofilms grown on lower water content

substrates presented a higher hydrophobicity and chemical stability than those from biofilms grown on higher water content substrates. Such fundamental knowledge on the biophysical features of amyloid fibrils sheds light on the influence of water on biofilm behavior and how the molecular structure of biofilm matrix defines biofilm macroscopic properties. Understanding the molecular behavior of the biofilm matrix formed in various growth conditions may inspire future strategies to engineer biofilm-based materials.

KEYWORDS: Amyloid fibers, Curli, Biofilm matrix, *E. coli*, Water, Spectroscopy

Graphical Abstract

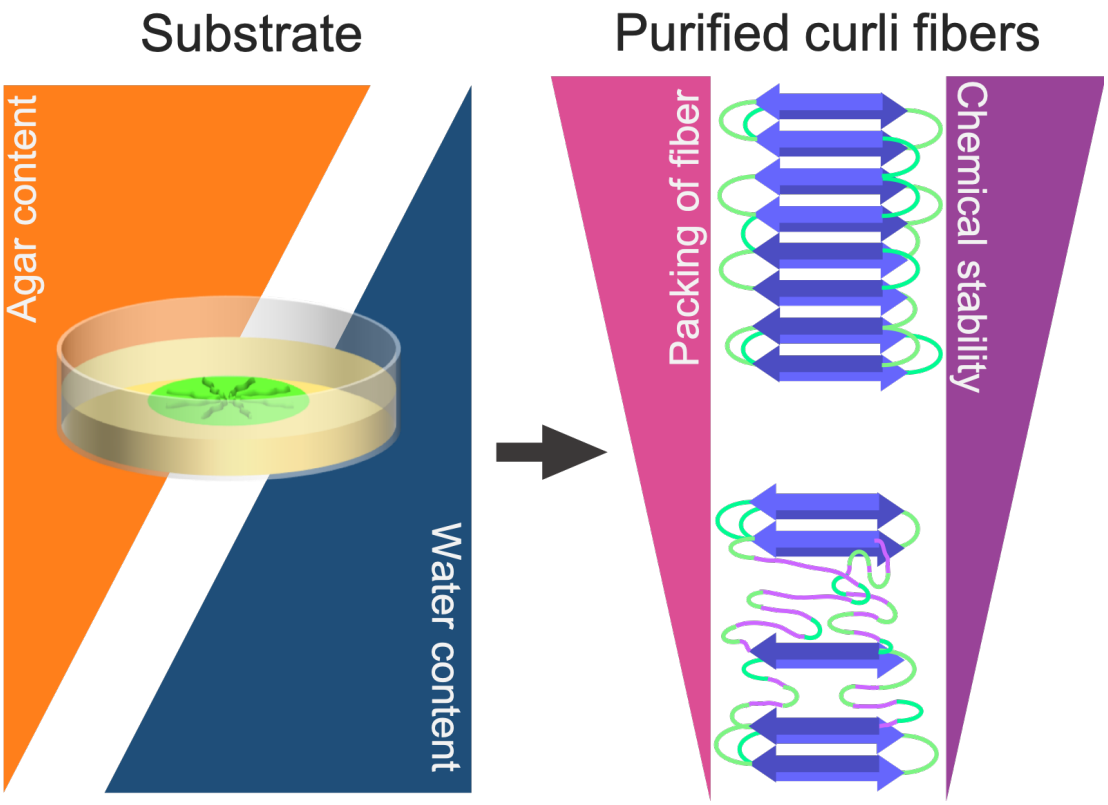

Biofilms are surface-associated groups of microbial cells that are embedded in a self-produced extracellular matrix (ECM). These living materials provide bacteria with resistance against environmental stresses such as exposure to antibiotics.[1–3] Within the biofilm, the ECM consists of a network of biopolymers, mainly made of polysaccharides, proteins, and nucleic acids. The shape and structure of a biofilm depend not only on the organism and the nature of the ECM components it produces,[4,5] but also on the growth medium and the growth conditions.[4,6] Indeed, biofilm morphogenesis is influenced by environmental cues such as the presence of salt, oxidative stress, charged surfaces and the water content substrate.[3,6–11] These parameters may also determine biofilm properties *via* different mechanisms. For example, the flux of water driven by osmotic gradients induces biofilm swelling as well as nutrient transport, which in turn governs bacteria proliferation and matrix production.[6,7,9] Moreover, the confinement of bacteria growth by the substrate influences biofilm density, gives rise to complex biofilm morphologies and thereby modulates bacterial access to nutrients. These processes have been proposed to determine several properties of the biofilms,[7,10,11] including their mechanical properties.[4,5,8,12] Even though the relation between bacteria environment and biofilm properties has been investigated macroscopically, the role of the microscopic organization of the biofilm matrix and the molecular structure of its components in this relation is still unclear. Yet, this piece of knowledge would be of fundamental interest both to leverage the full potential of biofilms as tunable biological materials and to develop strategies to prevent biofilm formation where they are detrimental, e.g. in medical and industrial contexts.[13–15]

Amyloid fibers, which are often found in biofilms proteinous ECM, is known as a common determinant of biofilm morphogenesis. The formation of amyloid fiber correlates with the growth rate of the biofilms and is required to yield robust biofilms.[7,12] Moreover, if their fibrillation is inhibited, the formation of the biofilm might not occur.[16] The main characteristics of amyloid fibers

are their intrinsic rigidity, polarity and charged nature.[17] These properties explain the growing interest for using amyloids as biological materials over the years. *Escherichia coli* (*E. coli*) is a common biofilm-forming bacterium that can be found in the digestive human track and has been domesticated as *E. coli* K-12 for wide lab uses.[2,7] While the ECM produced by wild type *E. coli* was recently shown to be made of both amyloid fibers and naturally modified cellulose,[11] amyloid fibers represent the major component.[1,2] The amyloid fibers formed by *E. coli*, also known as curli fibers, are biopolymers that are assembled extracellularly from csgA monomers.[18] CsgA is secreted as a soluble, unstructured protein to be converted to amyloid fiber using accessory proteins as a nucleator.[18,19] The amyloid fibrillation happens by addition of csgA to the extremity of the biopolymer.[18] The secondary structure is rich in β-sheets, a characteristic feature of amyloid fibers. This cross-β structure provides curli fibers with a notable rigidity and a remarkable stability that is further supported by the interactions of their side chains.[20] In the biofilm, the curli fibers form tangled networks in a basket-like manner around the cells.[3] Beside determining biofilm rigidity, curli fibers also contribute to the adhesion properties of the biofilm.[1,3,21] The mechanisms by which these fibers assemble and behave have been widely studied in aqueous solution, the main focus being to characterize the assembly and aggregation kinetics of the fibers. [7,18,22] Different biophysical techniques were used, namely circular dichroism,[7,18,22] infrared spectroscopy[18] and fluorescence spectroscopy.[7,22] Yet, much remains to be explored, in particular how the physico-chemical properties of the *E. coli* biofilm microenvironment influence the fibrillation of curli fibers and how this relates to the behavior of the biofilm as whole.

The present work aims at clarifying the role of curli fibers in the adaptation of biofilm properties to water availability during growth. To avoid additional interactions within the ECM, we used *E. coli* bacteria of the strain W3110, which produce curli fibers but no modified cellulose,[3] and

cultured them on nutritive substrates of different water contents. After 5 days of growth, we purified the curli fibers from the biofilms obtained in each condition and performed a comparative study of the final fiber conformation using well-established microscopy and spectroscopy techniques. This approach enabled us to demonstrate that the overall mass, the structure, and the properties of the curli fiber assembled in the *E. coli* biofilms depend on the availability of water during growth. Indeed, amyloid fibers purified from biofilms grown on substrate of low water content presented higher hydrophobicity and chemical stability than those obtained from biofilms grown on substrates of high-water content. These results highlight the versatility of the curli fibers and their key role in the adaptation of biofilms properties to the physicochemical cues of their environment. As such, this work will greatly benefit to the research aiming at engineering biofilm properties to make them a source of programmable living materials.

Results

To investigate the influence of water availability on the assembly of curli fibers in biofilms, *E. coli* from the strain W3110 were grown on salt-free Lysogenic Broth (LB) plates prepared with different agar contents (**Figure 1a**). In contrast to the *E. coli* strain AR3110 used in similar previous experiments and that produces a matrix made of both curli and phosphoethanolamine cellulose fibers,[8] the strain W3110 only produces curli fibers. A brief analysis of the macroscopic features (i.e. size, mass, water content and water uptake upon rehydration) was first conducted on the biofilms obtained in the different growth conditions. A purification protocol (see methods) was then applied to the different biofilm samples to harvest the curli fibers from the matrix. Finally, detailed structural and chemical characterizations were performed of the curli fibers using microscopy and spectroscopy techniques.

Substrate water content influences biofilm size, mass and composition

After 5 days of growth, the biofilms were observed in transmission with a stereomicroscope (**Figure 1a**). The biofilms cultured on 0.5 % agar substrates (i.e. on wet substrates) are significantly larger compared to biofilms grown in the other conditions (i.e. on dryer substrates), which did not differ in size for the different agar contents (1.0, 1.8 and 2.5 %) (**Figure S1**). Weighing the biofilms after harvesting them from the surface showed that the bacteria cultured on substrates with lower agar contents formed biofilms of significantly higher wet mass than on substrates with higher agar concentrations (**Figure 1b**). To assess the contribution of water in these differences, the samples were dried and weighed again (**Figure S1**). The estimated water contents revealed no significant differences between biofilms grown in the different conditions (**Figure 1c**) as they spanned from 74.11 % (biofilms grown on 2.5 % agar substrates) to 77.18 % (biofilms grown on 0.5 % agar substrates) with a relatively large variability. Upon overnight rehydration of these dried samples,

the biofilm material grown on 0.5 % agar substrates showed the apparent highest water-uptake (**Figure 1d**).

A standard purification process[22] was then applied to the biofilms grown on the substrates with different agar contents (i.e. different water contents) in order to isolate the curli fibers secreted by the bacteria to form the matrix (see method section). The purification yield, defined as the mass of curli fibers per gram of dry biofilm, was then estimated from the concentration of monomers csgA measured by absorbance after treatment of the fibers with urea (**Figure 1e**). Interestingly, the highest purification yield was obtained from biofilms grown on substrates containing 1.8 % agar, i.e. the standard condition used to grow biofilms in previous studies involving *E. coli*.[39] Both higher and lower agar concentrations in the substrate lead to biofilms containing less curli fibers. In particular, biofilms grown on substrates with 0.5 % and 2.5 % agar content respectively yielded 4.5 times and 2 times less curli fibers than those grown in standard conditions (1.8 %). Note that this trend follows the one obtained on the water uptake per gram of dry biofilm after rehydration (**Figure 1f**), where the dry mass is mostly made of dry curli and bacteria. The correlation between the amount of curli produced by the biofilm and the water uptake capacity of the ECM suggests an interesting role of curli fibers in biofilm swelling and water storage (**Figure 1g**).

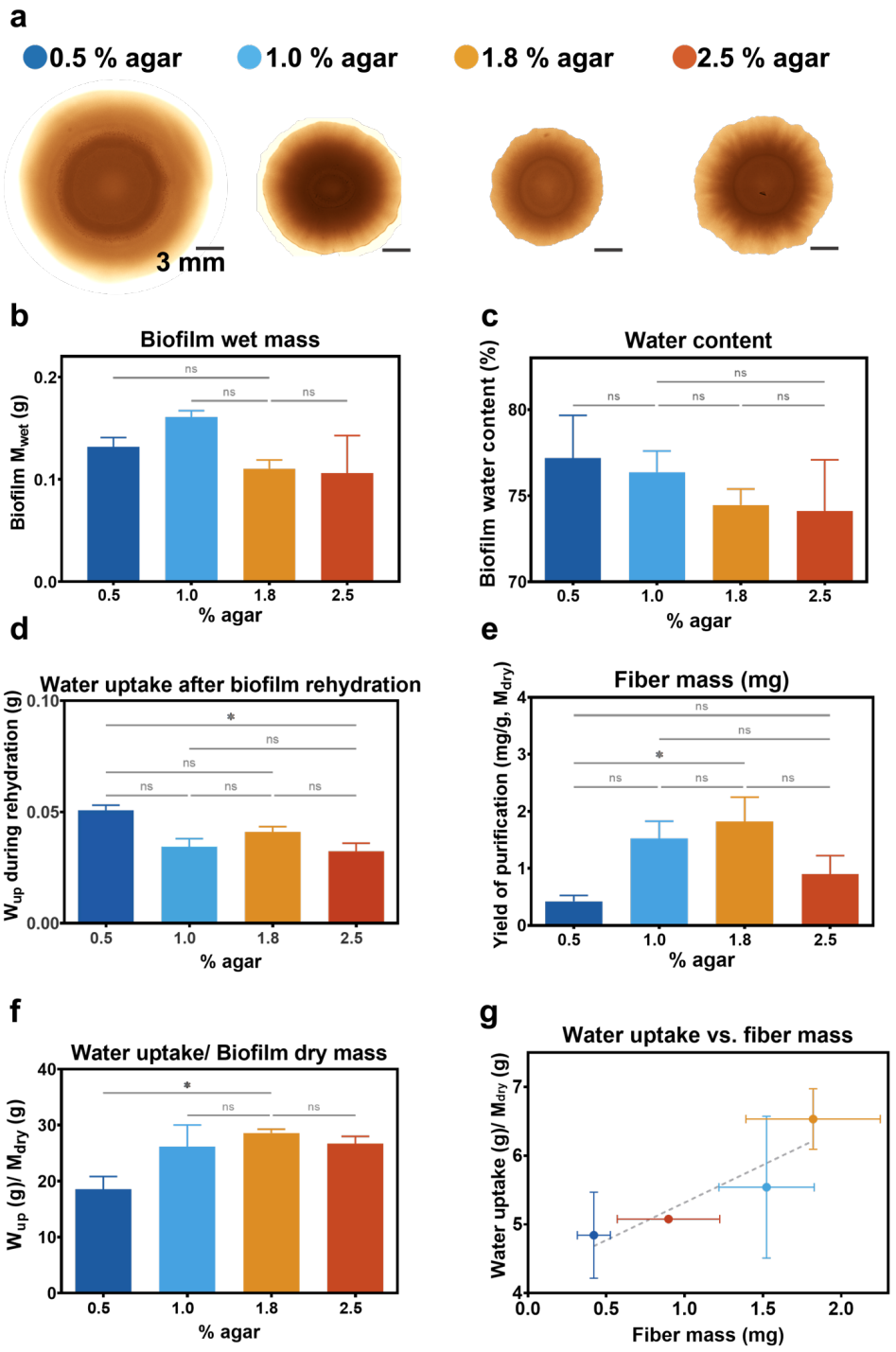

Figure 1 General characteristics of *E. coli* W3110 biofilms grown on substrates with different water contents. (a) Representative phenotype of five-days old biofilms grown on substrates with different water content. Scale bar= 3 mm. (b) Biofilm wet mass after scrapping them from the substrate and before purification. (c) Water content of biofilms calculated as $W = (m_{wet} - m_{dry})/m_{wet} \times 100\%$ w/w. (d) Water uptake per biofilm after overnight rehydration in excess of water. p value= ***. (e) Purification

yield of the curli fibers extraction process in milligram of csgA per gram of dry mass. The csgA content in the purified curli fibers was estimated by absorbance after denaturation using 8 M urea. p value= ***. (f) Water uptake per gram of biofilm dry mass. p value= *. (g) Water uptake of biofilms by fiber mass in each condition. N= 4 independent experiments.

To estimate how the water content of the substrate influences biofilm composition from these data, we considered the whole mass harvested from these *E. coli* W3110 biofilms to be the sum of the masses of i) the water, ii) the curli fibers and iii) the bacteria and remaining nutrients. The sum of the two latter is the dry mass of the biofilm (**Table 1**). Although all the growth conditions rendered biofilms with similar distribution of wet and dry mass (**Figure 1b**), there are some differences in the content of their dry masses (**Table 1**). Biofilms grown on lower water content substrates (2.5 % agar) present slightly higher content of dry mass. Both conditions, 0.5 % agar and 2.5 % agar, present lower content of curli in their dry mass composition than the other growth conditions.

Table 1 Composition of the *E. coli* W3110 biofilms grown on substrates of different water contents. The total mass corresponds to the sum of the water content and the dry mass. [a]The bacteria mass was estimated by substracting the curli mass given by the csgA quantification after purification from the dry mass. The percentages of bacteria and csgA are given with respect to the dry mass. N= 4 biofilms per experiments.

Growth condition	Units	Total mass	Water	Dry mass	csgA[a]	Bacteria[a]
0.5 % agar	mg	970.8 ± 121.27	715.47 ± 89.4	255.32 ± 32	0.207 ± 0.14	255.11 ± 31.88
	%	100	73.7	26.30	0.081 ± 0.06	99.2 ± 0.05
1.0 % agar	mg	1124.83 ± 44.34	839.01 ± 33.07	285.82 ± 11.27	0.436 ± 0.1	285.38 ± 11.23
	%	100	74.60	25.41	0.152 ± 0.03	99.85 ± 0.03
1.8 % agar	mg	771.5 ± 60.40	564.43 ± 44.20	207.07 ± 16.21	0.418 ± 0.11	206. ± 76 16
	%	100	73.16	26.84	0.146 ± 0.10	99.85 ± 0.10
2.5 % agar	mg	741.35 ± 257.82	517.31 ± 180	224.03 ± 78	0.184 ± 0.02	223.85 ± 78
	%	100	69.78	30.22	0.09 ± 0.03	99.9 ± 0.03

Curli fibers formed in biofilms grown on wet substrates reveal less β-sheet structures

To make sure that the purification yielded the expected product, the purified materials were examined by transmission electron microscopy (TEM), by fluorescence confocal microscopy after Thioflavin S (ThioS) staining and by Fourier transform infrared (FT-IR) spectroscopy (**Figures 2**). On the TEM images, all the samples appeared as needle-like structures of 11 to 13 nm width without significant differences (**Figure 2a**). This confirmed the presence of fibers. ThioS is a fluorescence probe that reports the presence of β- sheet pleated structures.[23] As the samples stained positive for ThioS, the amyloid nature of the fibers was confirmed as well (**Figure 2b**). [23] The difference in the ThioS intensity of the fibers suggested that biofilm growth conditions render fibers with different conformations (**Figure 2a-b**). In all the samples, agglomerated structures were detected and could be interpreted as clumps of tightly associated fibrils and protofibrils. These clumps remained after extended sonication prior to imaging, indicating strong adhesive forces linking the aggregates together.[18] The fluorescence intensity of the ThioS signal (relative to background) measured in the samples obtained from biofilms grown on 0.5 % agar substrates was significantly lower than in samples obtained from the other conditions (**Figure 2b**). To further assess the difference in structure of the fibers, we studied conformational characteristics by fluorescence studies (**Figure 2c**) and ATR-FTIR spectroscopy studies (**Figure 2d-e**)**.**

It has been demonstrated that ThioT fluorescence intensity is related to the number of exposed β-sheets, therefore reporting qualitive differences in fibrils packing. ThioT binds the β-sheets forming gutter-like structures running parallel to the amyloid fiber axis, which leads to characteristic changes of the ThioT spectrum.[24,25] Here, all fiber samples showed an increase of the ThioT intensity between 10 and 30 times compared to the original ThioT intensity (**Figure 2c**). Moreover, fibers assembled in the biofilms grown on the 0.5 % agar substrates present the lowest

β-sheet content. Therefore, we suggest that these amyloid-like β-sheets that differ in nature, extent and/or packing of their β-strands.[25]

The presence of the amyloid fibers was again confirmed by attenuated total reflectance Fourier transform infrared (ATR-FTIR) spectroscopy, which also gave further insights into their secondary structure. Indeed, this technique is widely used to study protein structure and is especially suited for amyloids.[25–27] The analysis was focused on the amide I′ band (from 1700 to 1600 cm^{-1}) that mostly represents the amide C=O stretching and is especially sensitive to protein secondary structure.[26–28] All the samples showed spectra similar to **Figure 2d**. The predominant band (**Figure 2d**, purple) was centered around 1620 cm^{-1} and assigned to β-sheet structures.[28] Indeed, a narrow and intense absorption band between 1615 and 1630 cm^{-1} is a hallmark for amyloid fibers as it indicates a large, planar and extremely well-ordered cross-β spine.[26,27,29] The second band located around 1660 cm^{-1} is usually assigned to β-turns structures (**Figure 2d**, green).[18,20,28] Finally, using band fitting to decompose the spectra into its overlapping components systematically revealed a minor contribution around 1650 cm^{-1}, which is assigned to random and α-helix structures (**Figure 2d**, pink). In the case of curli fibers purified from *E. coli* biofilms, the contribution of each of these two components could not be distinguished.

Despite the similarities among the samples, the detailed analysis of the secondary structure contents in the amide I' band showed significant differences in the packing of the curli fibers harvested from biofilms grown on the different agar substrates (**Figure 2e and S2**). For example, band decomposition reveals that fibers formed in biofilms grown on substrates with high water content (i.e. 0.5% agar) contain below 50 % of β-sheet while the fibers grown in the other conditions reach 60 %. However, the curli fibers from the 0.5 % agar conditions contain almost twice the amount of β-turns structures compared to the other fibers.

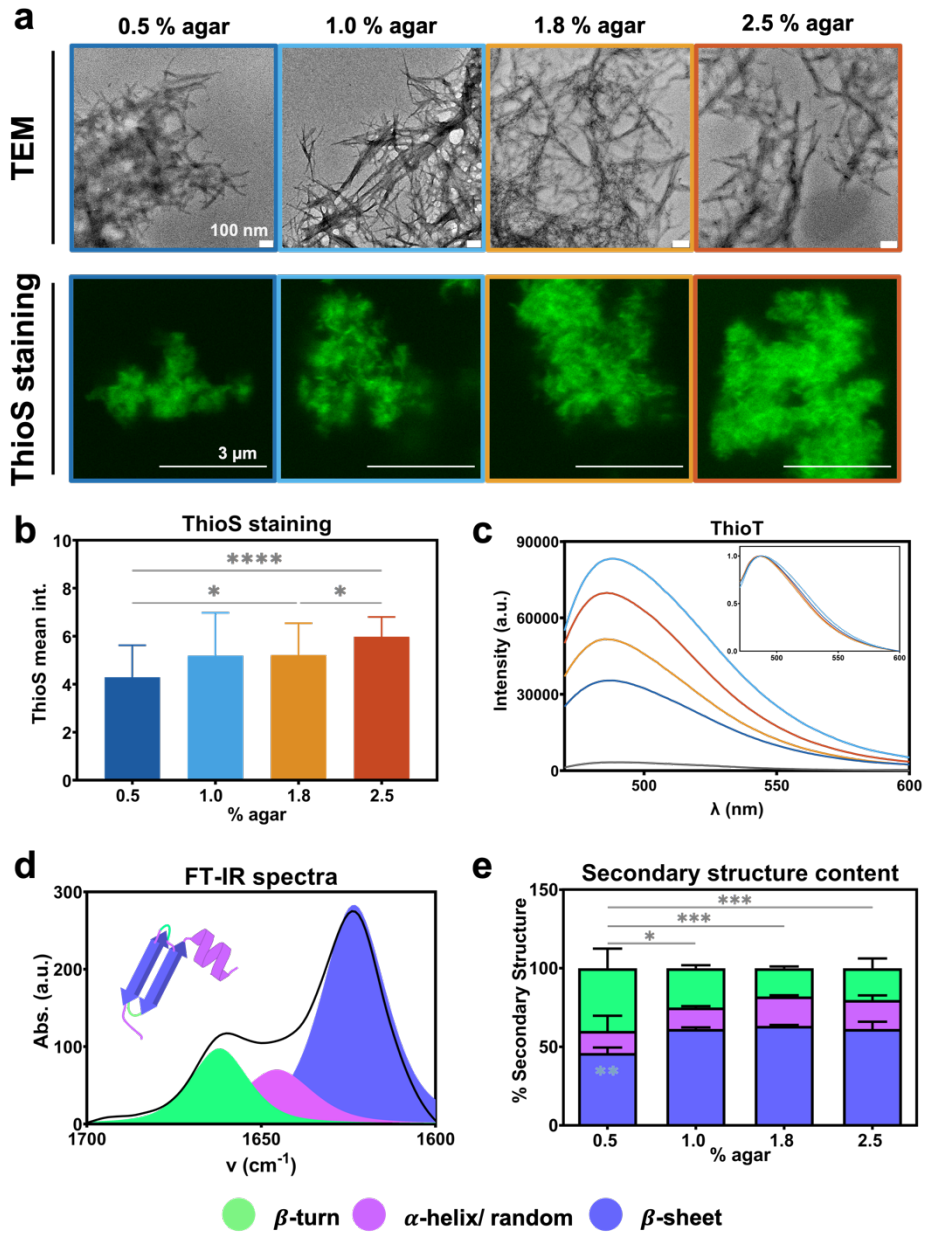

Figure 2 Identification of purified curli fibers from *E. coli* biofilms. (a) Transmission Electron Microscopy of purified curli fibers (top) and fluorescence confocal microscopy of purified curli fibers stained with Thioflavin S (bottom). (b) ThioS mean intensities of the stained purified fibers. p value= **. N= 5-10. (c) ThioT fluorescence emission spectra of the fibers at equivalent mass concentrations. N=4. (d) Representative FTIR absorbance spectrum obtained on curli fibers purified from *E. coli* biofilms grown on 1.8 % agar, focused on the Amide I' region. The spectra were fitted (color curves) using the 3 spectral components identified by second derivative on the Fourier self-deconvoluted spectra. p value= **. (e) Distribution of the 3 types of secondary structure in the curli fibers obtained in the different growth conditions. ***β***-turns components are significantly different when

compared to fibers grown on a 0.5 % agar, ***β***- sheet component of fibers in dry conditions (1.0, 1.8 and 2.5 % agar) are also significantly different to the dried condition fibers (Asterix in light blue). N= 4.

The hydrophobicity of the curli fibers depends on the substrate water content

To further detail the structural features and associated properties of the curli fibers obtained from biofilms grown in different conditions, we used the solvatochromic dye 1-anilinonaphthalene- 8-sulfonic acid (1,8-ANS). When alone, 1,8-ANS emits a weak fluorescence signal that both increases and shifts its maximum upon binding to hydrophobic pockets.[30] In the presence of each of the fibers tested, 1,8-ANS showed not only an increase in the intensity, but also a hyperchromic shift, suggesting a more hydrophobic environment for fibers fibrillated in dried conditions (**Figure 3a**). The phasor plot analysis helps to visualize the variations in the hydrophobicity of the fibers obtained in the different growth conditions (**Figure 3b**). In brief, the phasor analysis consists in a Fourier transform of the spectral information (or lifetime, see methods) into a two-dimensional space where the axes represent the real and imaginary components.[31,32] In this polar plot, the angle carries the information of the spectral center of mass and the radial direction carries the spectral width (See Figure S3 for more details).[31,32] The hydrophobicity increases clockwise, 1,8-ANS in buffer being the less hydrophobic sample. Fibers grown in dried conditions have the lowest hydrophobicity, while those grown in standard conditions have the highest hydrophobicity (**Figure 3b**). Upon estimating the increase of the 1,8-ANS fluorescence emission (**Figure 3c**), we observed a similar trend to that of the ThioT intensity variation (**Figure 3d**, derived from Figure 2c). ThioT and 1,8-ANS have different targets within the fibers: ThioT is incorporated to the β-sheets,[33] whereas 1,8-ANS binds to the exposed hydrophobic cavities of the fibers.[34,35] These results suggest that the β-sheet content might be responsible for the hydrophobicity in the fibers (**Figure 3c-d**). [18]

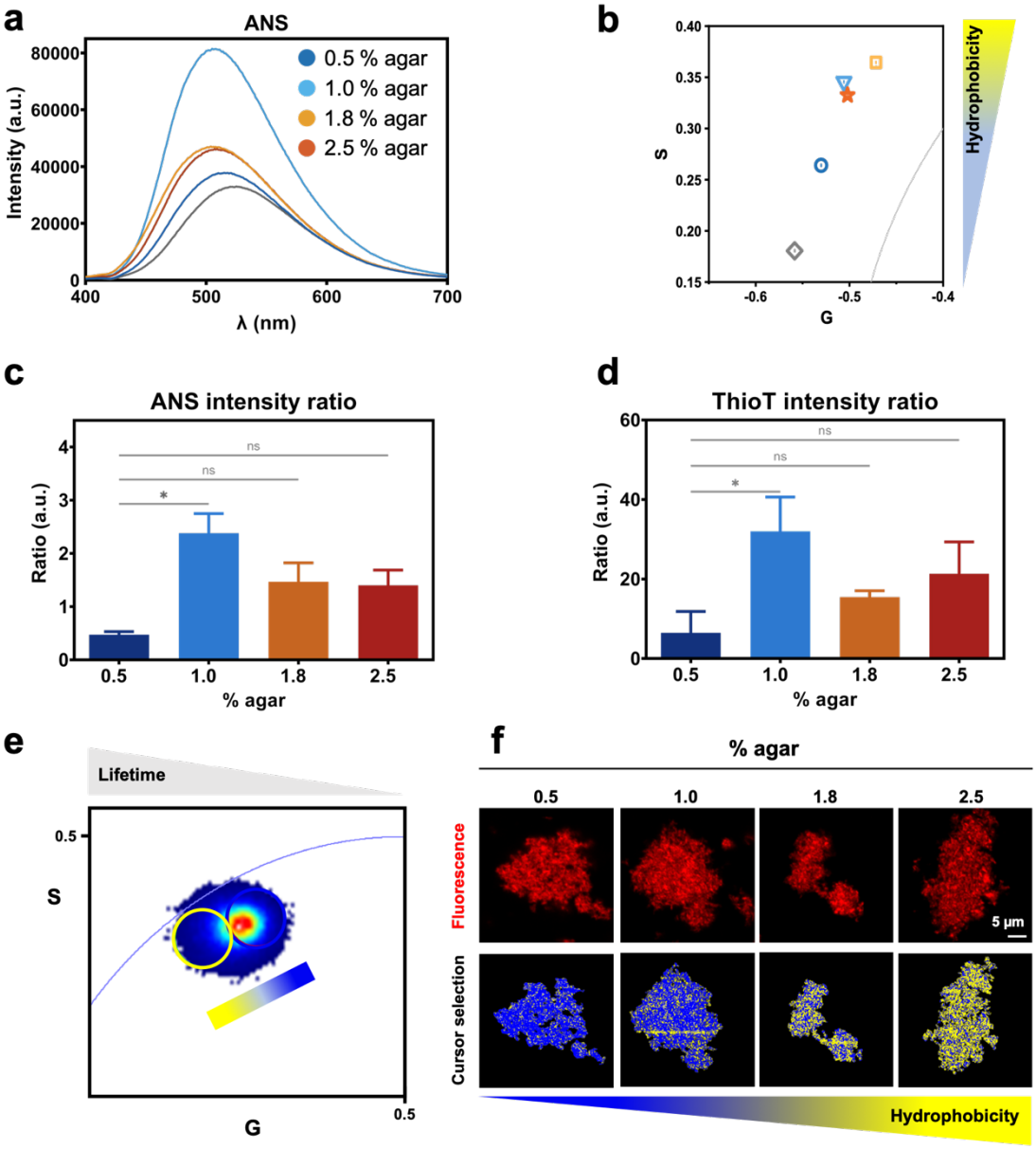

Figure 3 Hydrophobicity of curli fibers purified from *E. coli* biofilms grown on substrates of different water contents. (a) 1,8-ANS emission spectra in the presence of the fibers at equivalent mass concentration. Emission of 1,8-ANS in buffer is also included (grey). N= 4 - 5. (b) Phasor spectral plot of the purified samples bound to the probe 1,8-ANS. S and G correspond to the real and imaginary parts of the Fourier transform of the spectra (see methods). (c-d) Values describing the increase in intensity of the probes when bound to the purified fibers. Quantification of the increase was estimated by division of the area under the curve of each spectra of the probe (ANS or ThioT) with each fiber by the area under the curve of the emission spectra of the probe alone. p value=** (e) Nile Red lifetime phasor analysis. Phasor plot for the lifetime of the different purified fibers. (f) Confocal microscopy images of purified fibers stained with NR (top) and phasor map (bottom) in which each pixel is colored according to the color of

the corresponding cursor in the lifetime phasor plot in (e). The choice of the size and the position of the cursor is arbitrary and it is used to highlight average properties of the lifetime distributions.

Nile red (NR) is another solvatochromic dye sensitive to the fibers tertiary structure.[36] One of its main advantages is that it is fluorescent in the visible region of the spectra (λ_{em}=585 nm), making it convenient for fluorescence microscopy. Here we use a combined FLIM-phasor approach to assess the changes in NR lifetime within the fibers obtained in different biofilm growth conditions (see experimental section).[37–39] We show the representative confocal microscopy images of fibers stained with NR and the corresponding phasor plot for the lifetime of the fibers obtained from biofilms grown on the different substrates (**Figure 3e-f**). An increase in the lifetime of NR indicates a less polar, i.e. more hydrophobic environment.[40,41] By using colored cursors (blue and yellow circles), pixels of a given lifetime can be selected and the corresponding pixels are mapped back onto the image using the same color code (**Figure 3e**). In this case, the blue cursor corresponds to shorter lifetimes (more polar environments) and the yellow cursor to longer lifetimes (more hydrophobic environments). An increase in the agar concentration correlates with a higher lifetime of NR in the fibers (more yellow in **Figure 3f**). As such, changes in the NR lifetime, i.e. environment hydrophobicity, between the fibers obtained in different growth conditions can be easily identified without fitting procedures. A statistical quantification of these changes can be found in the supporting information (**Figure S4-5**).

The tryptophan population of all fibers is accessible to the solvent

In order to get more information on the supramolecular organization of the fibers, experiments on the intrinsic fluorescence of the purified fibers were conducted. Curli fibers are formed mainly by assembly of csgA monomers.[29] This protein contains a single tryptophan (Trp), four tyrosine, and three phenylalanine residues. It has been reported that when excited at 280 nm, the intensity

observed from the intrinsic fluorescence emission, is mainly due to the contribution of Trp in csgA(**Figure 4a**).[42] Its maximum emission position varies from a non-polar Trp inside globular proteins (307 nm) to a polar Trp in the protein surface in contact with free water molecules (353 nm), generally associated to unfolded proteins.[43] When we excite the purified fibers at 280 nm, a single maximum around 350 nm can be observed on the spectra (**Figure 4b**). The steady-state emission spectrum of fibers assembled in biofilms grown in standard growth conditions (1.8% agar) have the highest emission, whereas the fibers assembled in biofilms grown on substrates with high water content (0.5 % agar) present the lowest Trp emission.

The differences observed in the intensity of the purified fibers usually reflect changes in solvent accessibility of the side chains of aromatic amino acids. Hence, we explored the exposure of the Trp residues in each fiber using neutral and ionic dynamic fluorescence quenchers (**Figure 4c-d**), namely acrylamide (polar and uncharged) and iodine (highly hydrated, large and negatively charged). Acrylamide interacts with all surfaces, regardless of their charge and is able to diffuse into the interior of proteins, thus providing information on the environment of surface-accessible and less-exposed Trp residues.[44] On the other hand, the iodide ion is limited to quenching Trp residues lying on or near the protein surface and its action depends on the surface charge adjacent to the indole moiety.[44] N-acetyl-L-tryptophanamide (NATA) was used as reference for the maximum quenching possible (**Figure 4c-d insets**).

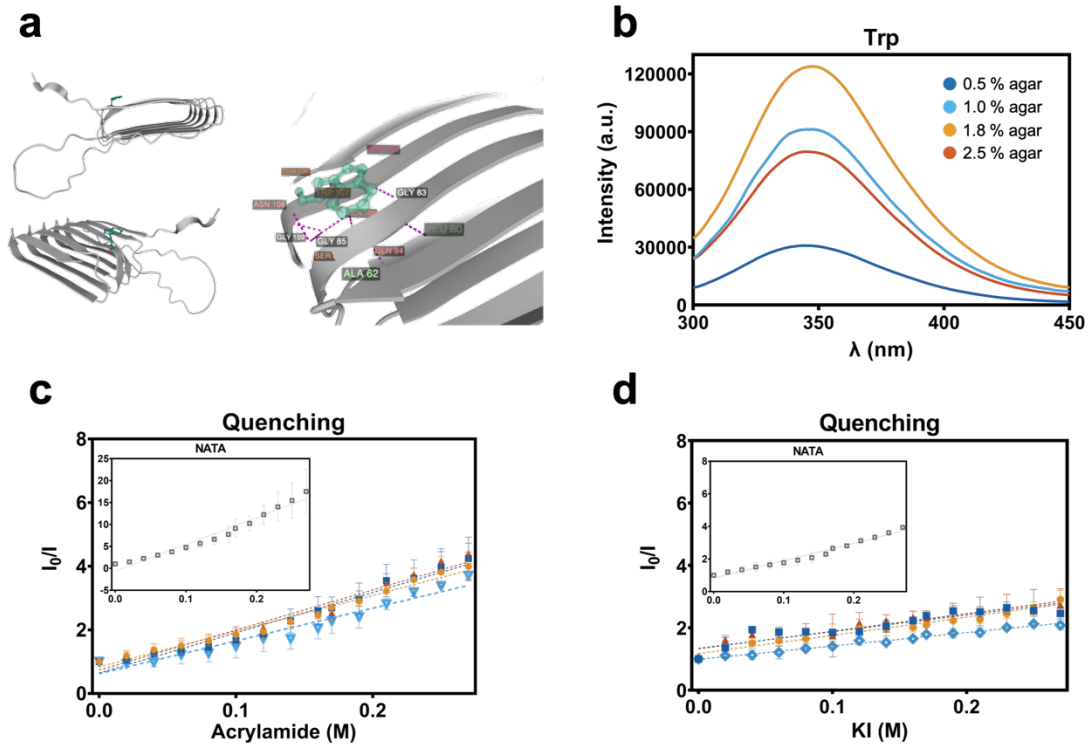

Figure 4 Characterization of the intrinsic Trp emission fluorescence of the purified curli fibers. (a) Position of the Trp[107] residue in the csgA protein as predicted by Alphafold. The residues interacting with Trp[107] are also depicted. (b) Intrinsic Trp emission fluorescence spectra of the fibers at equivalent mass concentrations (λ_{exc}= 280 nm). The inset depicts the normalization between 0-1 of the spectra for better comparison of the maxima position. Stern-Volmer plots of (c) acrylamide or (d) iodine quenching of Trp residues in the purified curli fibers. I_0 correspond to the emission signal of ThioT incubated with fibers at the beginning of the experiment (urea concentration= 0M). The insets show the effect of each quencher on NATA (grey). N= 4.

The Stern–Volmer plots showed no upward curvature, meaning that the quenching effect in all cases was predominately dynamic quenching, i.e. that fluorescence deactivation occurs because of the collision of the quencher with the fluorophore and not because of a binding interaction between both molecules.[44,45] Moreover, the addition of the quencher (acrylamide or iodide), even at high concentrations did not induce a shift in the spectra of the Trp in the purified fibers (**Figure S6**). This suggests that there is no alteration of the hydrophobic character of the fibers throughout the experiment.

Quenching experiments indicated no buried Trp residue within the fibers (**Figure 4c-d**).[46] The plots of the ratio between the fluorescence intensities in the absence and the presence of quenchers (I/I_0) as a function of the quencher concentration yielded straight lines under all external conditions within the concentration range 0–0.4 M. There are no significant differences for the value of the quenching slopes (K_{sv} values) of the purified fibers: all values are between 10 – 12 M^{-1} (**Table S1**). Of note, the K_{sv} values for acrylamide are much lower than those obtained with NATA denoting that the emitters are not exposed to the solvent in the fibers and imply rapid diffusion of the quencher to the Trp.[44,46] These results suggest that the Trp population of the fiber is near the surface.

Chemical stability of curli fibers increases when grown in dry conditions

To study the implications of the structural differences described above, we tested the thermal and chemical stability of the purified fibers against exposure to a temperature slope and different urea concentrations (**Figure 5**).

Thermal denaturation was performed by heating the fibers from 25 to 80°C and cooling them down back to 25°C. At each temperature step, the structure of the fibers was monitored using ATR-FTIR spectroscopy. All the samples of fibers showed a remarkable stability, with no significant change of structure as monitored by band analysis (**Figure 5a-d**).

The chemical stability of the fibers was tested against increasing urea concentrations from 0.1 to 8M (**Figure 5e-f**). The presence of amyloid fibers was monitored by the fluorescence intensity emitted by ThioT (**Figure 5e**). The stability of the fibers significantly decreased as the water content of the corresponding biofilm the substrate increased (**Figure 5f**).

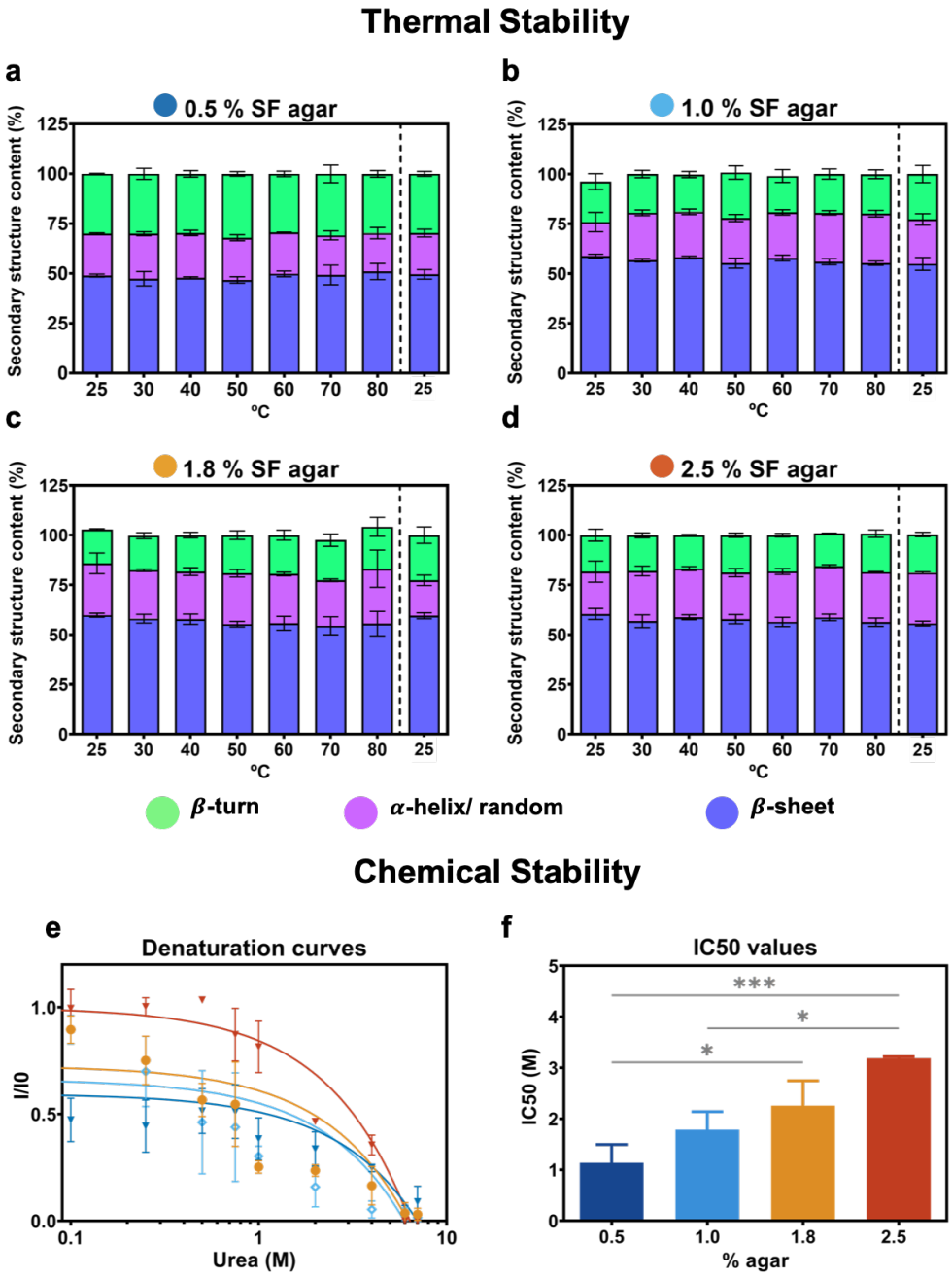

Figure 5 Stability of the purified curli fibers. (a-d) Thermal stability of the fibers purified from biofilms grown on substrates of different water contents. Secondary structure content by analysis of FTIR spectra of the curli fibers treated with increasing temperatures (25 – 80 °C). The data after the dashed line represents the secondary structure content of fibers after a sudden decrease of temperature (from 80 – 25 °C). N= 3. (e-f) Chemical stability of the purified fibers upon denaturation with increasing urea concentrations (0.1 – 8 M). The presence of the fibers was observed by ThioT fluorescence emission intensity. I_0 corresponds to

the ThioT emission when bound to fibers without urea in the solution. IC50 corresponds to the urea concentration at which the ThioT intensity is 50 % of the initial one. p value= *** N= 4.

Discussion

In vitro studies have previously showed that external conditions such as molecular crowding, temperature and pH affect the fibrillation of amyloids and their final conformation.[4,18,25] The present work focuses on curli amyloid fibers purified from *E. coli* biofilms and demonstrates that their physical-chemical properties depend on the water availability in the biofilm growth environment. Indeed, electronic microscopy, FT-IR and fluorescence spectroscopy revealed differences in the yield of curli fibers purified from the biofilms, in the packing of these fibers, their hydrophobicity and their chemical stability.

Water plays an important role during the different stages of protein aggregation in fiber formation. It can favor the interactions between hydrophobic regions of the monomers or between polyglutamine sequences, and lead to structure variations when trapped inside proteins.[47,48] The more crowded the environment, the more probable the protein hydration shells will change and thereby the aggregation of the amyloid proteins.[25,48] The packing differences measured in curli fibers purified from biofilms grown on substrates with different water contents are consistent with such changes (**Figure 2d-e**). These structural differences in the fibers are further supported by the differences observed in tryptophan (Trp) emission signal, which reflect differences in Trp interactions with surrounding groups such as threonine (Thr), aspartic acid (Asp), glutamine (Gln), and asparagine (Asn) (**Figure 4a**).[25,43] Indeed, these polar and charged residues have the ability to quench Trp fluorescence. A change in the packing of the fibers or a change in the structure surrounding the Trp could give way to different ways of interaction between the Trp and these residues. Hence, the lower intensity in the spectra of fibers obtained under wet conditions (0.5 %

agar) can be further explained by changes in the structure of these fibers. The position of the maximum wavelength of Trp emission suggests that the environment of Trp is relatively polar and structureless (**Figure 4b**), indicating that Trp is probably located near the surface of the fibers, as indicated for the monomer according to the Alpha-fold prediction (Figure 4a).[43]

The fibers obtained from biofilms grown on substrates with high water content (0.5 % agar) also showed lower hydrophobicity, as estimated with the 1,8-ANS and the NR probes (**Figure 3b-f**).[30] Interestingly, the phasor plot obtained from 1,8-ANS spectra revealed that the fibers purified from biofilms grown on standard substrates (1.8 % agar) present more hydrophobic patches exposed to the surface (**Figure 3a-b**). Moreover, the similar trends of the ThioT and the 1,8-ANS intensities as a function of growth condition, suggest that the β-sheet content can be correlated to the hydrophobicity in the fibers.[18] NR fluorescence studies confirmed that fibers obtained in wet conditions are less hydrophobic than fibers obtained in dry conditions (**Figure 3e-f**). The difference between the results obtained from the 1,8-ANS and the NR experiments on the 1.8 % agar may be attributed to the different binding mechanisms of the probes.[35,49,50] Nonetheless, both results indicate structural differences between fibers fibrillated in dry and wet conditions.

Amyloids are highly ordered and arranged into intermolecular β-sheets and cross β-structures, which contain many strong hydrogen bonds that enhance the overall stability of the fibers.[18,51] Models of curli fibers also suggest that the hydrogen bonds between Gln and Asn residues from different monomers form a network that contributes to the stability of these fibers.[18,19,29] Considering the importance of the structure-function relationship in proteins, the implications of the structural differences observed in the purified curli fibers were assessed with stability assays. While all fibers showed high stability against thermal denaturation,[17] their stability upon urea exposure revealed significant differences (**Figure 5a-d**). The thermal stability can be attributed to the high content of

β-sheets in fibers obtained from all conditions (**Figure 2e**). However, the relatively lower β-sheets content measured in curli fibers obtained at high water concentrations (0.5 % agar, **Figure 2e**), could explain their lower chemical stability compared to those obtained on dryer substrates (**Figure 5e-f**). Indeed, less densely packed fiber structures not only result in weaker interactions between the distant Gln and Asn residues, but they also provide better access for urea to denature the fibers by interactions with their hydrophobic and amide groups (**Figure 6**).[52] Note that the fibers extracted from biofilms grown on 0.5% agar not only contain less than 50% of β-sheet but almost twice as much β-turns compared to the other conditions (**Figure 2e**), which indicates that β-turn structure is less chemically stable than β-sheet.

Previous studies involving different bacteria strains showed that biofilms grown on substrates with high water content (e.g. 0.5 % agar) have a less dense matrix which is heterogeneously distributed across the biofilm thickness.[5,8] Our results would attribute these observations to a lower production of curli fibers in these conditions (**Figure 1e, Table 2**). By affecting the quantity of curli fibers in the biofilm matrix as well as their molecular structure (**Figure 2e**), the water content of the agar substrate is therefore expected to affect biofilm macroscopic features like their growth kinetics[7] and their mechanical properties.[3,5,10] For example, the high content of β-turns in the curli fibers purified from biofilm grown on substrates with high water content (0.5 % agar) results in a lower packing compared to the fibers obtained from dryer conditions (1.0 – 2.5 % agar) (**Figure 2e**). Such difference in structure could be explained by larger average spacings between strands (**Figure 6**), and the resulting flexibility of the curli fibers in the matrix could further contribute to the lower rigidity of biofilms grown on wet substrates.[8]

The biofilms grown in the extreme conditions used in our experiments (0.5% and 2.5% agar) not only contained less curli, but this curli content also appeared to correlate with the rehydration

capacity of the dried biofilms (**Figure 1f-g**). These results suggest that, in addition to providing biofilms with adhesion and rigidity,[3,8] curli fibers also promote biofilm water uptake from the surroundings. This ability constitutes a significant advantage for biofilms growing at solid-air interfaces, i.e. in environments where an influx of water carries the nutrients from the substrate to the biofilm. While osmotic gradients have been proposed to be involved in this transport, their origin is yet not clear.[6] Since bacteria are able to regulate the number and location of the curli fibers formed[7], and since less curli fibers were found in the biofilms grown in wet conditions than those grown in dryer conditions (**Figure 1e**), curli production could be proposed as a way for bacteria to create these osmotic gradients in conditions where water is more difficult to reach. The discrepancy of this hypothesis with the lower quantity of curli fibers measured in biofilms grown on the driest substrates (2.5 % agar) could be explained by the extreme difficulties to reach the nutrients, which could impair the overall biofilm growth and/or matrix production. Changing the water content of the substrate was also proposed to affect biofilm size *via* a partial confinement resulting from the friction along the surface[6]. For example, biofilms grown on substrates with a high water content spread more than biofilms grown on dryer substrates due to the lubricating effect of water (**Figure S1**).[8] In this context, one could question if such confinement also affects the assembly of the curli fibers. Further studies will focus on clarifying if the water content of the substrate influences the molecular assembly of curli fibers in *E. coli* biofilms by affecting the nutrient transport or the confinement of the growth on the surface.

Overall, such knowledge about the molecular structure – function relationship of the biofilm matrix not only helps to better understand the role of water in the assembly of amyloid fibers and the role of curli fibers in *E. coli* biofilm physiology, but also contributes to uncover the full

potential of biofilms as engineered living materials, which can become construction materials, sustainable plastic-like materials or scaffolds for tissue engineering.[13–15]

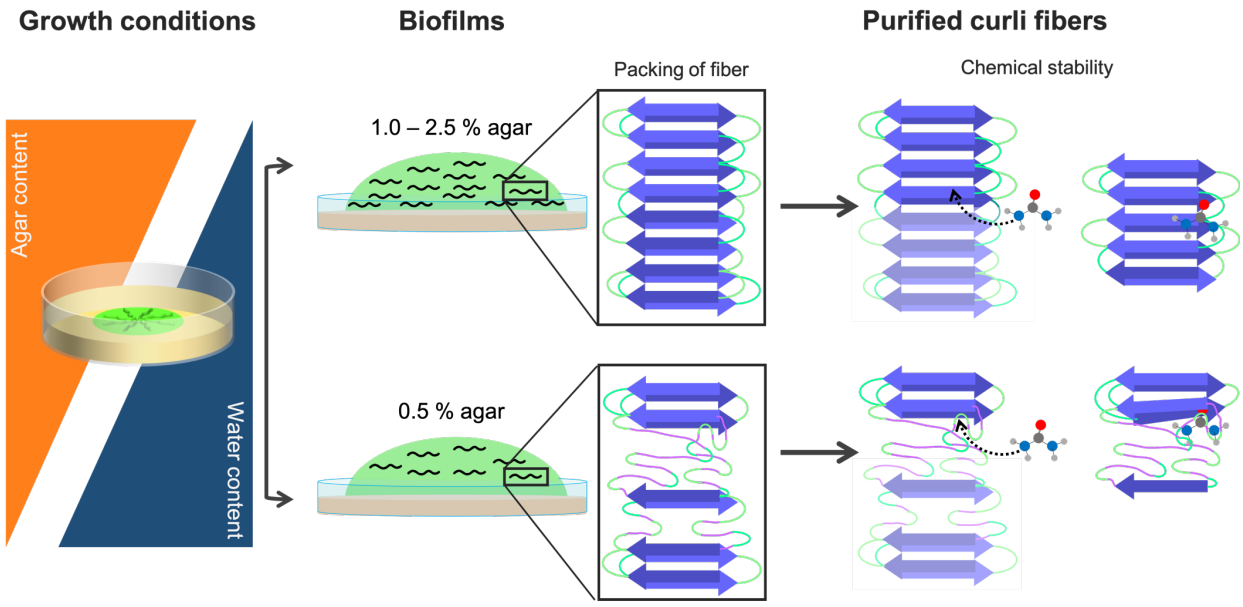

Figure 6 A graphical interpretation of the results. By varying the water content in the substrates used for biofilm growth, we showed a dependence of the production of curli fibers. The packing of the fibers also varies as a function of the substrate water content, which in turn influences their interactions with denaturants like urea.

Experimental Section

Bacterial strain and growth

The biofilm-forming bacterial strain *E. coli* K-12 W3110 was used throughout this study. Salt-free agar plates (15mm diameter) were prepared with 0.5%, 1.0%, 1.8%, or 2.5% w/v of bacteriological grade agar–agar (Roth, 2266), supplemented with 1% w/v tryptone (Roth, 8952) and 0.5% w/v yeast extract (Roth, 2363). Each plate was inoculated with arrays of 9 drops of 5µL of bacterial suspension (OD_{600} ~0.5 after 10x dilution). The suspension was prepared from a single colony and grown overnight in Luria–Bertani (LB) medium at 37°C with shaking at 250 rpm. After inoculation, the excess of water evaporated from the drops and left bacteria-rich disks of

comparable sizes from 4 to 8mm diameter, depending on the growth condition. Biofilms were grown for 5 days in total (~120h).

Biofilm imaging

Three biofilms per condition were imaged with a stereomicroscope (AxioZoomV.16, Zeiss, Germany) using the tiling function of the acquisition software (Zen 2.6 Blue edition, Zeiss, Germany). To estimate the biofilm size, 3 independent biofilms were measured at their equatorial line using the Fiji software.[53] An average was then calculated for each growth condition.

Biofilm dry mass and water uptake

The water content and water uptake of the biofilms were determined by scrapping 7 biofilms per condition from the respective agar substrates after 5 days of growth (~120 h). Biofilms were placed in plastic weighing boats and dried at 60°C for 3 h in an oven. Wet and dry masses (m_{wet}, m_{dry}) were determined before and after drying.[8] To determine the water uptake (W_{up}), we added Millipure water in excess (5 ml) to the biofilms harvested from each condition, covered them with aluminum foils to avoid evaporation and left overnight. The water excess was removed and the biofilm samples were weighed again (m_{rewet}). The biofilms water content in each growth condition was estimated with **Eq. (1)**

Eq. (1) $W = (m_{wet} - m_{dry})/m_{wet} \times 100\%$ w/w

The water uptake of biofilms after rehydration was determined with **Eq. (2)**

Eq. (2) $W_{up} = m_{rewet} - m_{dry}$

All procedures were carried out in four independent experiments.

Curli fiber purification

Fiber purification involved a similar process as reported in previous works.[22] Briefly, a total of 27 biofilms (~ 1g of biofilm material) were scraped from the surface of the substrates. Biofilms were blended five times on ice with an XENOX MHX 68500 homogenizer for 1min at 2-min intervals. The bacteria were pelleted by centrifuging two times at low speed (5000g at 4°C for 10min). A final concentration of NaCl 150 mM was added to the supernatant and the curli pelleted by centrifuging at 12.000g at 4°C for 10 minutes. The pellet was resuspended in 1mL of solution containing 10mM tris (pH 7.4) and 150mM NaCl, and incubated on ice for 30min before being centrifuged at 16.000g at 4°C for 10 minutes. This washing procedure was repeated thrice. The pellet was then resuspended in 1mL of 10mM tris solution (pH 7.4) and pelleted as described above (16.000g at 4°C for 10 minutes). The pellet was again suspended in 1mL of 10mM tris (pH 7.4) and centrifuged at 17.000g at 4°C for 10 minutes. This washing step was repeated twice. The pellet was then resuspended in 1mL of SDS 1% v/v solution and incubated for 30min. The fibers were pelleted by centrifuging at 19.000g at 4°C for 15min. The pellet was resuspended in 1mL of Milli-Q water. This washing procedure was repeated thrice. The last resuspension was done in 0.1mL of Milli-Q water supplemented with 0.02% sodium azide. The fiber suspension was stored at 4°C for later use. The protein concentration in monomeric units of the suspensions was determined by the absorbance from an aliquot incubated in 8M urea at 25°C for 2h, a treatment leading to complete dissociation of the fibrils as verified by Thioflavin T measurements.

Transmission electron microscopy (TEM)

2µL drops of fiber suspension were adsorbed onto Formvar-coated carbon grids (200 mesh), washed with Milli-Q water, and stained with 1%(w/v) uranyl acetate. The samples were imaged in a JEOL-ARM F200 transmission electron microscope equipped with two correctors for imaging

and probing. For the observations, we applied an acceleration voltage of 200 kV. The width of the purified fibers values in TEM images were measured using the scale tool of the GATAN GMS 3 software. To avoid subjectivity over 10 different images and over 10 identified fibers per field were used.

Fluorescence confocal microscopy

5µM fiber samples were incubated with 0.2mg/mL Thioflavin S (ThioS) for 2h at room temperature under stirring. The fibers were then washed twice by alternating centrifugation and resuspension in Milli-Q water to remove the excess of ThioS. The fibers were finally observed under a LEICA confocal microscope SP8 FALCON (Leica, Mannheim, Germany) with a water immersion 62X objective (1.2NA) under excitation at 405nm in the emission range 415-550 nm. To estimate the ThioS mean intensity in each fiber, five images were analyzed: different points in the fiber region were taken and the signal normalized according to the background signal, an average was then estimated. This procedure was performed five times in each image analyzed.

Attenuated total reflectance Fourier transform infrared spectroscopy (ATR-FTIR)

IR spectra were acquired on a spectrophotometer (Vertex 70v, Bruker Optik GmbH, Germany) equipped with a single reflection diamond reflectance accessory continuously purged with dry air to reduce water vapor distortions in the spectra. Fibers in Milli-Q water samples (~10µL) were spread on a diamond crystal surface, dried under N_2 flow to obtain the protein spectra. A total of 64 accumulations were recorded at 25°C using a nominal resolution of $4cm^{-1}$.

Spectra were processed using Kinetic software developed by Dr. Erik Goormaghtigh at the Structure and Function of Membrane Biology Laboratory, Université Libre de Bruxelles, Brussels, Belgium. After subtraction of water vapor and side chain contributions, the spectra were baseline

corrected and area normalized between 1700 and 1600cm^{-1} (Figure S2). For a better visualization of the overlapping components arising from the distinct structural elements, the spectra were deconvoluted using Lorentzian deconvolution factor with a full width at the half maximum (FWHM) of 20 cm^{-1} and a Gaussian apodization factor with a FWHM of 30 cm^{-1} to achieve a line narrowing factor K = 1.5.[28] Second derivative was performed on the Fourier self-deconvoluted spectra for band assignment. The bands identified by both procedures were used as initial parameters for a least square iterative curve fitting of the original IR band (K = 1) in the amide I' region, using mixed Gaussian/Lorentzian bands. Peak positions of each identified individual component were constrained within ±2 cm^{-1} of the initial value.

Table 2 FWHH input values in cm−1 and their physically plausible ranges expected for each type of secondary structure[25,26,28]

Secondary structure component		FWHH input (cm^{-1})	Lower limit (cm^{-1})	Upper limit (cm^{-1})
β-sheet	High wavenumber component	9	8	11
	Low wavenumber component	17	14	19
	α-helix/ random	20	5	30
	Turns	20	5	30

Fluorescence spectroscopy

Corrected steady-state emission spectra were acquired with a FluoroMax®-4 spectrofluorometer (HORIBA). Spectra were recorded at 25°C using a 3-mm path cuvette (Hellma® Analytics). ThioT measurements were performed at final concentrations of 3 μM protein, 1 mM probe in Glycine buffer, pH 8.2, using λ_{exc} = 446 nm and spectral bandwidths of 10 nm. 1-anilino-nafthalene-8-sulfonate (1,8-ANS) emission spectra were obtained after 30 min incubation at room temperature of mixture containing 5 μM protein and 100 μM dye in the corresponding buffer, using λ_{exc} = 370 nm and bandwidth of 5 nm. Intrinsic fluorescence spectra (5 μM protein) were acquired using λ_{exc}= 280 nm and 5/5 nm slit bandwidths.

For quenching experiments, increasing volumes of 5 M acrylamide or potassium iodide (KI) were added to a 4 µM fiber suspension, 4 µM N-Acetyl-L-tryptophanamide (NATA, Sigma-Aldrich) solution or buffer alone until reaching a maximum quencher concentration of 0.37 M. Spectra were recorded after 5 min incubation using λ_{exc} = 280 nm. Blank substracted spectra were corrected for dilution and inner filter effects by multiplication with a factor of $10(A_{exc}+A_{em})/2$, thereby compensating for the absorption of KI and acrylamide at the fluorescence excitation and emission wavelength. Quenching curves were fit by linear regression with the Stern-Volmer equation (**Eq. (3)**)

Eq. (3) $I_0/I = 1 + K_{sv}[Q]$

where I_0 and I are the fluorescence intensities in the absence and in the presence of quencher, respectively, at the concentration [Q] and K_{sv} is the dynamic quenching constant.

Thermal stability assay

5µM fiber samples were incubated at 25, 30, 40 ,50 60, 70 and 80°C for 3 min before their measurement with ATR-FTIR spectroscopy. An extra measurement was done by taking the fibers from 80°C to a bath water at 25°C and incubate the samples there for 3 min. Data were acquired as described above.

Chemical stability assay

To test the chemical stability of the protein fibers, 5 µM samples were prepared by incubation of increasing urea concentration (0 – 8 M) and left for 2 h at room temperature to ensure equilibrium. Thioflavin T (ThioT) was then added in a final concentration of 1 mM and fluorescence emission spectra of the samples were acquired under excitation at λ_{exc} = 446 nm and spectral bandwidth of 5 nm. Emission of the ThioT in urea was done and no significant signal was detected.

The IC50 value was estimated by fitting the data to a linear regression (Y = a * X + b) and then calculating IC50 = (0.5 - b)/a.

Fluorescence Lifetime Imaging Microscopy (FLIM)

Two-photon excitation of Nile red was performed at 860 nm with a pulsed Ti:Sapphire laser with 80Hz repetition rate (Spectra-Physics Mai Tai, Mountain View, CA). The image size was 512x512 pixels, the pixel size was 75 nm and the detection range were 600 to 728 nm. FLIM calibration of the system was performed by measuring the known lifetime of the fluorophore Coumarin 6 in ethanol.[37] For these experiments, 5 μM fibers where placed in clean glass and 5 μM of NR was added.

Phasor analysis

Spectral phasor plots were used to visualize 1,8-ANS spectral shifts. The phasor plots are 2D scatter graphs, where the axes are the real (G) and imaginary (S) components of the Fourier transform of the fluorescence spectra. This transformation offers a powerful, model free, graphic method to characterize spectral[31] and lifetime information.[54] A detailed analysis can be found elsewhere.[37,55,56] In this work, ANS spectra can be transformed using the following for x and y coordinates:

Eq. (4) $$y = G_{(\lambda)} = \frac{\sum_\lambda F(\lambda)\cos\left(\frac{2\pi n(\lambda-\lambda_0)}{L}\right)}{\sum_\lambda F(\lambda)}$$

Eq. (5) $$x = S_{(\lambda)} = \frac{\sum_\lambda F(\lambda)\sin\left(\frac{2\pi n(\lambda-\lambda_0)}{L}\right)}{\sum_\lambda F(\lambda)}$$

where $F(\lambda)$ are the fluorescence intensity values, λ_0 is the initial wavelength of the spectrum (λ_0 =400 nm), L is the length of the spectrum and n is the harmonic value. The values L=300 (from 400 to 700 nm) and n=1 were used for phasor calculations. The angular position of the phasor in the plot is related to the center of mass, while the radial position depends on the full width at half maximum of the spectrum. Spectral phasor plots were constructed using Originlab data analysis software.

The FLIM phasor analysis allows the transformation of the fluorescence signal from each pixel in the image to a point in the phasor plot. FLIM data were processed using SimFCS, an open source software developed at the Laboratory of Fluorescence Dynamics, Irvine, California (available at http://www.lfd.uci.edu). Further details of FLIM phasor analysis are provided in S4.

Statistical analysis

For statistical analysis, a Shapiro Wilk test was carried out for normality of the data. Fall data was analyzed using a Kruskal-Wallis non-parametric test (alpha= 0.05) was performed where p= 0.0008, save for experiments in Figure 2. The latter had no normal distribution, and were analyzed using a One-way ANOVA (alpha= 0.05) where p= 0.007.

Supporting Information

The following files are available free of charge:

- Figure S1: Biofilm general features (size and dry mass)
- Figure S2: Amide I' spectra of curli fibers purified from *E. coli* biofilms
- Figure S3: Spectral phasor plot analysis
- Figure S4: Lifetime phasor plot analysis
- Figure S5: Nile red FLIM analysis
- Figure S6: Effect of quenching experiments in the spectra of curli fibers
- Table S1: Stern Volmer constants of quenching experiments

AUTHOR INFORMATION

Corresponding Author

*Macarena Siri: *Macarena.Siri@mpikg.mpg.de*

Author Contributions

The manuscript was written through contributions of all authors. All authors have given approval to the final version of the manuscript.

ACKNOWLEDGMENT

M.S. acknowledges support from the Max Planck Queensland Centre on the Materials Science for Extracellular Matrices and A.M acknowledges support from the Alexander von Humboldt foundation. The authors also thank Christine Pilz-Allen for her technical support in the laboratories, Peter Werner and Heike Runge for their help in doing the transmission electronic microscopy experiments, and Peter Fratzl and Ricardo Ziege for the useful discussions throughout

this study. The authors are also grateful to Regine Hengge (HU Berlin) for providing the *E. coli* strain W3110 and to Eric Goormaghtigh from the SFMB group at the Université Libre de Bruxelles for providing the Kinetics Software.

REFERENCES

1. Jeffries, J., Fuller, G. G. & Cegelski, L. Unraveling Escherichia coli 's Cloak: Identification of Phosphoethanolamine Cellulose, Its Functions, and Applications . *Microbiol. Insights* **12**, 117863611986523 (2019).
2. Jeffries, J. *et al*. Variation in the ratio of curli and phosphoethanolamine cellulose associated with biofilm architecture and properties. *Biopolymers* **112**, 1–11 (2021).
3. Serra, D. O., Richter, A. M. & Hengge, R. Cellulose as an architectural element in spatially structured escherichia coli biofilms. *J. Bacteriol.* **195**, 5540–5554 (2013).
4. Chen, D. *et al*. Characteristics and influencing factors of amyloid fibers in S. mutans biofilm. *AMB Express* **9**, 1–9 (2019).
5. Zeng, G. *et al*. Functional bacterial amyloid increases Pseudomonas biofilm hydrophobicity and stiffness. *Front. Microbiol.* **6**, 1–14 (2015).
6. Trinschek, S., John, K., Lecuyer, S. & Thiele, U. Continuous versus Arrested Spreading of Biofilms at Solid-Gas Interfaces: The Role of Surface Forces. *Phys. Rev. Lett.* **119**, 1–5 (2017).
7. Andreasen, M. *et al*. Physical determinants of amyloid assembly in biofilm formation. *MBio* **10**, 1–12 (2019).
8. Ziege, R. *et al*. Adaptation of Escherichia coli Biofilm Growth, Morphology, and Mechanical Properties to Substrate Water Content. *ACS Biomater. Sci. Eng.* **7**, 5315–5325 (2021).
9. Ryzhkov, N. V., Nikitina, A. A., Fratzl, P., Bidan, C. M. & Skorb, E. V. Polyelectrolyte Substrate Coating for Controlling Biofilm Growth at Solid–Air Interface. *Adv. Mater. Interfaces* **8**, (2021).
10. Lembré, P., Di Martino, P. & Vendrely, C. Amyloid peptides derived from CsgA and FapC modify the viscoelastic properties of biofilm model matrices. *Biofouling* **30**, 415–426 (2014).
11. Thongsomboon, W. *et al*. Phosphoethanolamine cellulose: A naturally produced chemically modified cellulose. *Science (80-.).* **359**, 334–338 (2018).
12. Romero, D., Aguilar, C., Losick, R. & Kolter, R. Amyloid fibers provide structural integrity to Bacillus subtilis biofilms. *Proc. Natl. Acad. Sci. U. S. A.* **107**, 2230–2234 (2010).
13. Nguyen, P. Q., Botyanszki, Z., Tay, P. K. R. & Joshi, N. S. Programmable biofilm-based materials from engineered curli nanofibres. *Nat. Commun.* **5**, 1–10 (2014).
14. Axpe, E. *et al*. Fabrication of Amyloid Curli Fibers-Alginate Nanocomposite Hydrogels with Enhanced Stiffness. *ACS Biomater. Sci. Eng.* **4**, 2100–2105 (2018).
15. Duraj-Thatte, A. M. *et al*. Water-processable, biodegradable and coatable aquaplastic from engineered biofilms. *Nat. Chem. Biol.* **17**, 732–738 (2021).
16. Cegelski, L. *et al*. Small-molecule inhibitors target Escherichia coli amyloid biogenesis and biofilm formation. *Nat. Chem. Biol.* **5**, 913–919 (2009).
17. Knowles, T. P. J. & Mezzenga, R. Amyloid fibrils as building blocks for natural and artificial functional materials. *Adv. Mater.* **28**, 6546–6561 (2016).
18. Dueholm, M. S. *et al*. Fibrillation of the major curli subunit CsgA under a wide range of conditions implies a robust design of aggregation. *Biochemistry* **50**, 8281–8290 (2011).
19. Wang, X. & Chapman, M. R. Curli provide the template for understanding controlled amyloid propagation.

Prion **2**, 57–60 (2008).

20. Evans, M. L. & Chapman, M. R. Curli biogenesis: Order out of disorder. *Biochim. Biophys. Acta - Mol. Cell Res.* **1843**, 1551–1558 (2014).
21. Kikuchi, T., Mizunoe, Y., Takade, A., Naito, S. & Yoshida, S. I. Curli fibers are required for development of biofilm architecture in Escherichia coli K-12 and enhance bacterial adherence to human uroepithelial cells. *Microbiol. Immunol.* **49**, 875–884 (2005).
22. Chapman, M. R. *et al*. Role of Escherichia coli curli operons in directing amyloid fiber formation. *Science (80-.).* **295**, 851–855 (2002).
23. Sun, A., Nguyen, X. V. & Bing, G. Comparative analysis of an improved thioflavin-S stain, Gallyas silver stain, and immunohistochemistry for neurofibrillary tangle demonstration on the same sections. *J. Histochem. Cytochem.* **50**, 463–472 (2002).
24. Nagaraj, M. *et al*. Predicted Loop Regions Promote Aggregation: A Study of Amyloidogenic Domains in the Functional Amyloid FapC. *J. Mol. Biol.* (2020) doi:10.1016/j.jmb.2020.01.044.
25. Siri, M., Herrera, M., Moyano, A. J. & Celej, M. S. Influence of the macromolecular crowder alginate in the fibrillar organization of the functional amyloid FapC from Pseudomonas aeruginosa. *Arch. Biochem. Biophys.* **713**, 109062 (2021).
26. Sarroukh, R., Goormaghtigh, E., Ruysschaert, J. M. & Raussens, V. ATR-FTIR: A 'rejuvenated' tool to investigate amyloid proteins. *Biochim. Biophys. Acta - Biomembr.* **1828**, 2328–2338 (2013).
27. Moran, S. D. & Zanni, M. T. How to get insight into amyloid structure and formation from infrared spectroscopy. *J. Phys. Chem. Lett.* **5**, 1984–1993 (2014).
28. GOORMAGHTIGH, E., CABIAUX, V. & RUYSSCHAERT, J. -M. Secondary structure and dosage of soluble and membrane proteins by attenuated total reflection Fourier-transform infrared spectroscopy on hydrated films. *Eur. J. Biochem.* **193**, 409–420 (1990).
29. Barnhart, M. M. & Chapman, M. R. Curli biogenesis and function. *Annu. Rev. Microbiol.* **60**, 131–147 (2006).
30. Gohlke, J. R. the most popular fluorescence probes in use at this time . Weber. (1972).
31. Fereidouni, F., Bader, A. N. & Gerritsen, H. C. Spectral phasor analysis allows rapid and reliable unmixing of fluorescence microscopy spectral images. *Opt. Express* **20**, 12729 (2012).
32. Malacrida, L. & Gratton, E. LAURDAN fluorescence and phasor plots reveal the effects of a H2O2 bolus in NIH-3T3 fibroblast membranes dynamics and hydration. *Free Radic. Biol. Med.* **128**, 144–156 (2018).
33. Krebs, M. R. H., Bromley, E. H. C. & Donald, A. M. The binding of thioflavin-T to amyloid fibrils: Localisation and implications. *J. Struct. Biol.* **149**, 30–37 (2005).
34. Hawe, A., Sutter, M. & Jiskoot, W. Extrinsic fluorescent dyes as tools for protein characterization. *Pharm. Res.* **25**, 1487–1499 (2008).
35. Scheibel, T. & Serpell, L. *Physical Methods for Studies of Fiber Formation and Structure. Protein Folding Handbook* vol. 1 (2008).
36. Mishra, R., Sjölander, D. & Hammarström, P. Spectroscopic characterization of diverse amyloid fibrils in vitro by the fluorescent dye Nile red. *Mol. Biosyst.* **7**, 1232–1240 (2011).
37. Digman, M. A., Caiolfa, V. R., Zamai, M. & Gratton, E. The phasor approach to fluorescence lifetime imaging analysis. *Biophys. J.* **94**, 14–16 (2008).
38. Sancataldo, G., Anselmo, S. & Vetri, V. Phasor-FLIM analysis of Thioflavin T self-quenching in Concanavalin amyloid fibrils. *Microsc. Res. Tech.* **83**, 811–816 (2020).
39. Chung, C. W. *et al*. Label-Free Characterization of Amyloids and Alpha-Synuclein Polymorphs by Exploiting Their Intrinsic Fluorescence Property. *Anal. Chem.* **94**, 5367–5374 (2022).
40. Levitt, J. A., Chung, P.-H. & Suhling, K. Spectrally resolved fluorescence lifetime imaging of Nile red for measurements of intracellular polarity. *J. Biomed. Opt.* **20**, 096002 (2015).

41. Golini, C. M., Williams, B. W. & Foresman, J. B. Further Solvatochromic, Thermochromic, and Theoretical Studies on Nile Red. *J. Fluoresc.* **8**, 395–404 (1998).

42. Shu, Q. *et al.* The E. coli CsgB nucleator of curli assembles to β-sheet oligomers that alter the CsgA fibrillization mechanism. *Proc. Natl. Acad. Sci. U. S. A.* **109**, 6502–6507 (2012).

43. Ladokhin, A. S. Fluorescence Spectroscopy in Peptide and Protein Analysis. *Encycl. Anal. Chem.* 1–18 (2000) doi:10.1002/9780470027318.a1611.

44. Eftink, M. R. & Ghiron, C. A. Fluorescence quenching studies with proteins. *Anal. Biochem.* **114**, 199–227 (1981).

45. Jiskoot, W., Hlady, V., Naleway, J. J. & Herron, J. N. Application of fluorescence spectroscopy for determining the structure and function of proteins. *Pharm. Biotechnol.* **7**, 1–63 (1995).

46. Stevenson, S. G. & Preston, K. R. Intrinsic fluorescence and quenching studies of gluten proteins. *Cereal Chem.* **71**, 155–158 (1994).

47. Thirumalai, D., Reddy, G. & Straub, J. E. Role of water in protein aggregation and amyloid polymorphism. *Acc. Chem. Res.* **45**, 83–92 (2012).

48. Stephens, A. D. & Kaminski Schierle, G. S. The role of water in amyloid aggregation kinetics. *Curr. Opin. Struct. Biol.* **58**, 115–123 (2019).

49. Matulis, D. & Lovrien, R. 1-Anilino-8-Naphthalene Sulfonate Anion-Protein Binding Depends Primarily on Ion Pair Formation. *Biophys. J.* **74**, 422–429 (1998).

50. Sackett, D. L. & Wolff, J. Nile red as a polarity-sensitive fluorescent probe of hydrophobic protein surfaces. *Anal. Biochem.* **167**, 228–234 (1987).

51. Dandurand, J. *et al.* Conformational and thermal characterization of a synthetic peptidic fragment inspired from human tropoelastin: Signature of the amyloid fibers. *Pathol. Biol.* **62**, 100–107 (2014).

52. Zou, Q., Habermann-Rottinghaus, S. M. & Murphy, K. P. Urea effects on protein stability: Hydrogen bonding and the hydrophobic effect. *Proteins Struct. Funct. Genet.* **31**, 107–115 (1998).

53. Schindelin, J. *et al.* Fiji: An open-source platform for biological-image analysis. *Nat. Methods* **9**, 676–682 (2012).

54. Jameson, D. M., Gratton, E. & Hall, R. D. The measurement and analysis of heterogeneous emissions by multifrequency phase and modulation fluorometry. *Appl. Spectrosc. Rev.* **20**, 55–106 (1984).

55. Ranjit, S., Malacrida, L., Jameson, D. M. & Gratton, E. Fit-free analysis of fluorescence lifetime imaging data using the phasor approach. *Nat. Protoc.* **13**, 1979–2004 (2018).

56. Malacrida, L., Ranjit, S., Jameson, D. M. & Gratton, E. The Phasor Plot: A Universal Circle to Advance Fluorescence Lifetime Analysis and Interpretation. *Annu. Rev. Biophys.* **50**, 575–593 (2021).